
Simply Stabilizing the Loop via Fully Looped Transformer

Rao FU

Hong Kong Baptist University
csraofu@comp.hkbu.edu.hk

Zixuan YANG

Jilin University
zxyang25@mails.jlu.edu.cn

Jiankun ZHANG

Jilin University
jiankun24@mails.jlu.edu.cn

Jing MA

Hong Kong Baptist University
maging@comp.hkbu.edu.hk

Hechang CHEN

Jilin University
chenhc@jlu.edu.cn

Yu LI

Jilin University
liy90@jlu.edu.cn

Yi CHANG

Jilin University
yichang@jlu.edu.cn

Abstract

Scaling model performance typically requires increasing model size. Looped Transformer offers a compelling alternative by iteratively reusing the same Transformer blocks, trading additional computation for improved performance without increasing parameter count or context length. Because the number of loop iterations can be adjusted at inference, it also provides a natural mechanism for balancing performance and test-time compute. However, Looped Transformer still suffers from training instability when the number of loop iterations increases. Our analysis reveals that this instability stems from two sources: gradient oscillation and residual explosion. To address these two problems, we propose the Fully Looped Transformer, which introduces two parameter-free modifications: (1) Fully Looped Architecture, which distributes inter-loop signals across all layers to mitigate residual explosion; (2) Attention Injection, which reuses the existing attention block to suppress gradient oscillation. These modifications stabilize training dynamics, enabling the Fully Looped Transformer to be trained stably up to 12 loop iterations, whereas other baseline looped models collapse in this regime. In milder settings where Looped Transformer does not collapse, Fully Looped Transformer still improves average downstream-task performance by up to 13.2%. Overall, our experiments demonstrate that Fully Looped Transformer improves training stability, enhances downstream performance, and provides preliminary adaptability under different test-time compute budgets by varying loop iterations at inference.

1 Introduction

Large language models (LLMs) demonstrate excellent generalization capabilities across numerous downstream tasks through pretraining on massive text corpora from the internet. However, this scaling paradigm is increasingly constrained by the limited supply of high-quality public text data. According to the Chinchilla scaling law [Hoffmann et al., 2022], model parameters and training data should scale proportionally. Simply increasing model size without a corresponding increase in data leads to suboptimal training results. Meanwhile, Villalobos et al. [2024] show that the stock of public human-generated text data available for LLM pretraining grows at only 10% per year, while the dataset sizes used in practice have been growing at approximately $2.4\times$ per year. This growing

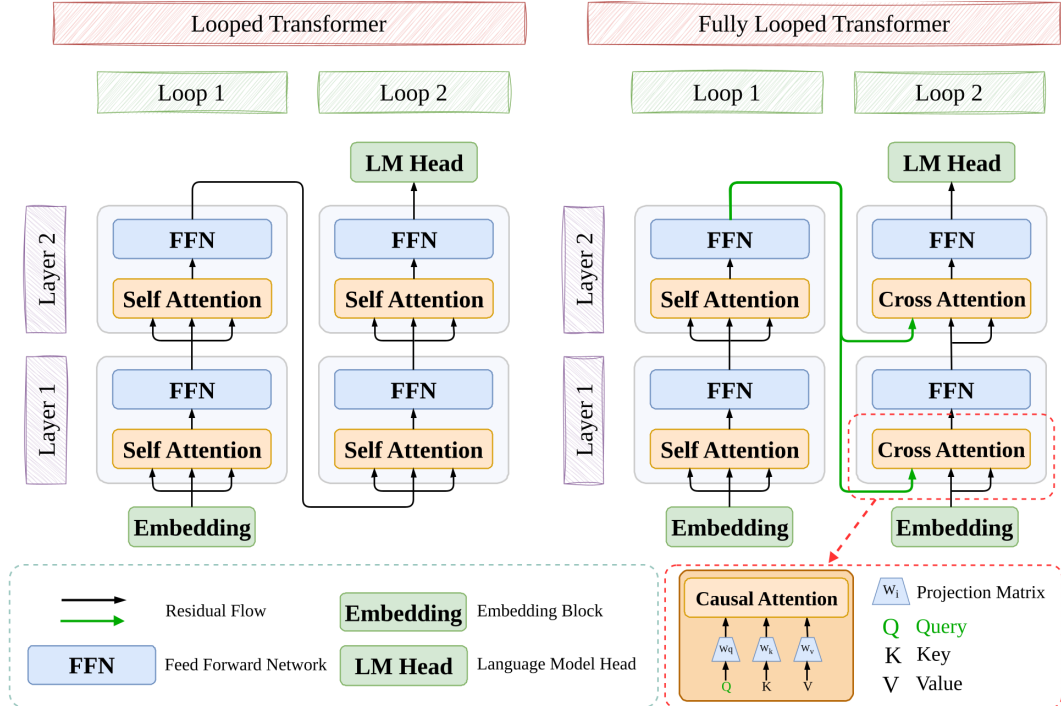


Figure 1: The comparison of Looped Transformer (LT) and Fully Looped Transformer (FLT). FLT uses **Fully Looped Architecture**, where all layers participate in the loop, and employs **Attention Injection** to reintroduce the residual flow generated in the previous iteration into the model by reusing the Self-Attention block as a Cross-Attention block. We use the causal mask in all attention blocks.

mismatch between data availability and computational capacity calls for new paradigms that can convert excess compute into performance gains without relying on ever-larger datasets.

Several research directions have been explored to address this challenge. One line of work focuses on improving data quality through rephrasing entire corpora [Niklaus et al., 2026], but this approach still fundamentally depends on the availability of high-quality data. Another promising direction is test-time scaling, where reinforcement learning is used to elicit extended chain-of-thought reasoning [Wei et al., 2023] at inference time [team et al., 2024, Guo et al., 2025]. Despite its strong empirical performance, this paradigm often increases the context length and inference cost substantially.

A complementary way to convert additional computation into performance is to provide the model with a looping mechanism. Looped Transformer [Giannou et al., 2023] follows this direction by iteratively reusing the same Transformer backbone blocks. Instead of increasing the model parameter count or expanding the context window, it unrolls the same shared blocks for multiple loop iterations. By virtue of the looping mechanism, Looped Transformer is parameter-efficient [Saunshi et al., 2025], naturally compatible with test-time compute adjustment [Koishekenov et al., 2025] and excels at reasoning tasks [Saunshi et al., 2025].

However, despite these advantages, Looped Transformer remains difficult to train when the number of loop iterations becomes large [Geiping et al., 2025, Zhu et al., 2025]. We also observe the same issue in our experiments: simply increasing the loop iterations of Looped Transformer can lead to training collapse. This motivates us to examine the training dynamics of Looped Transformer. Our diagnosis identifies two instability patterns. First, gradients can oscillate strongly during the early stage of training. Second, the residual-state norm can grow rapidly as loop iterations increase. We refer to these two phenomena as gradient oscillation and residual explosion, respectively.

Based on this diagnosis, we propose the **Fully Looped Transformer**, a simple parameter-free improvement of Looped Transformer. It consists of two modifications: (1) **Fully Looped Architecture**, which distributes the recurrent signal to all layers and mitigates residual explosion, and (2) **Attention Injection**, which reuses the existing attention block to inject recurrent information in a controlled

manner and suppress gradient oscillation. Together, these two modifications stabilize training without introducing additional learnable parameters.

Our main contributions are three-fold: (1) We diagnose the training instability of Looped Transformer and identify two associated phenomena: gradient oscillation and residual explosion. (2) We propose the Fully Looped Transformer, a simple yet effective improvement that can be trained stably without adding any parameters. (3) Through loop-scaling and ablation experiments, we show that Fully Looped Transformer trains stably in regimes where baseline looped models collapse, improves downstream-task average performance by up to 13.2%, and provides preliminary evidence of adaptability to different inference-time compute budgets. Our code is available at GitHub.

2 Related Work

2.1 Weight-Sharing Models

Many recurrent or looped language models can be conceptualized as weight-sharing architectures, leveraging a foundational technique to enhance parameter efficiency in deep neural networks. Universal Transformer [Dehghani et al., 2019] first extends this idea to the Transformer architecture by repeatedly applying the same backbone network across layers, enabling models to perform iterative refinement and endowing Transformers with the ability to simulate general computational processes. Looped Transformer [Giannou et al., 2023] simplifies this idea by using a more general decoder-only Transformer architecture. A large body of existing work [Saunshi et al., 2025, Geiping et al., 2025, Koishekenov et al., 2025] has demonstrated the significant advantages of Looped Transformer in test-time scaling and reasoning tasks. Concurrently, Parcae [Prairie et al., 2026] tried to address looped model instability via a dynamical systems framework to constrain the spectral norm of the residual state. In contrast, our work introduces a general architectural modification that requires no additional learnable parameters or computational overhead, allowing it to be integrated into existing Transformer architectures [Vaswani et al., 2023] with minimal changes.

2.2 Training Difficulties in Recurrent Models

Training difficulties in deep recurrent models are long-standing, with the most critical being the gradient explosion and vanishing gradient problems. Bengio et al. [1994] systematically pointed out that when training recurrent networks using backpropagation through time (BPTT), the gradient signal decays or explodes exponentially with each time step, making it difficult for the model to learn long-range dependencies. Pascanu et al. [2013] further analyzed the sources of this problem theoretically and proposed mitigation strategies such as gradient clipping. LSTM [Hochreiter and Schmidhuber, 1997] and GRU [Cho et al., 2014] introduced gating mechanisms to address this issue, effectively alleviating the problem by selectively filtering and controlling the information flow. However, in the context of Looped Transformer, these challenges persist. Because the model uses a shared-weight looped structure, it is essentially equivalent to an extremely deep recurrent network, making gradient stability a core challenge in training once again.

3 Diagnosing the Instability of Looped Transformer

Previous studies show that increasing the number of loop iterations can substantially make LT harder to train [Geiping et al., 2025, Zhu et al., 2025], but they do not explain the cause of such instability. To investigate this failure mode, we examine the early training dynamics of LT before full convergence. In our diagnostic runs, the relevant instability already appears during the early stage of optimization, so we use the first 2000 optimizer steps as a diagnostic window¹. In Figure 2, we compare LT models with 6, 9, and 12 loop iterations using the same 6-layer Transformer backbone, and include a 12-loop Fully Looped Transformer (FLT) as a stable control. All models use the same pretraining setup. We monitor three quantities: training loss, residual-state norm, and gradient L2 norm of the first FFN block. Additional experiment results and training details are provided in Appendix A.1.1 and A.2.

We define training collapse as a failure mode where the model can no longer produce a usable checkpoint for evaluation. In practice, this includes entering a persistent high-loss plateau, showing

¹This window is used only to identify the onset and persistence of training instability; final performance comparisons are conducted with fully trained models in Section 5.

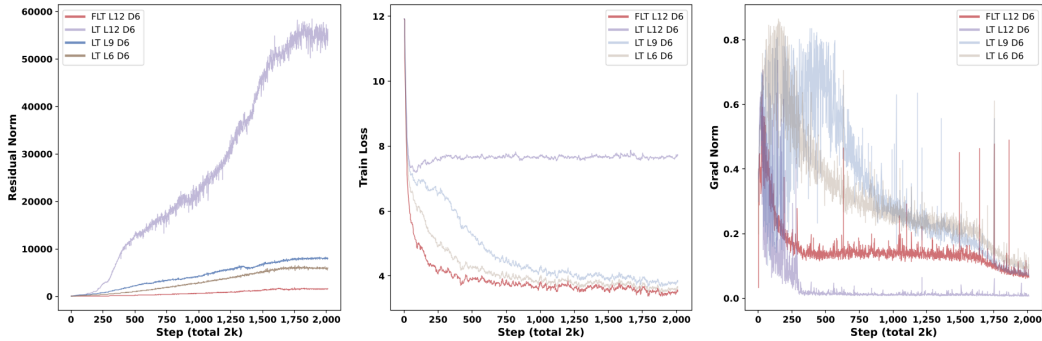


Figure 2: Training dynamics of LT and FLT during the first 2000 optimizer steps. **Left:** residual-state norm. **Middle:** training loss, smoothed with a factor of 0.9 for readability. **Right:** gradient L2 norm of the first FFN block.

severe loss fluctuations, or producing validation performance that is unusable. Under this definition, the 12-loop LT collapses in the early diagnostic run: after an initial decrease, its training loss stops improving and remains at a high plateau, while its residual-state norm continues to increase. Beyond this collapsed case, the loss curves also reveal a milder but consistent optimization difficulty for LT. As the number of loop iterations increases from 6 to 9, LT does not immediately collapse, but a clear loss gap emerges: the 9-loop LT maintains a higher training loss than the 6-loop LT throughout most of the diagnostic window. This indicates that increasing the loop count already makes optimization harder even before an outright high-loss plateau appears. In contrast, the 12-loop FLT remains stable throughout the same 2000 steps window, with smoother loss reduction, smaller residual-state norms, and more stable gradient dynamics. Based on these observations, we propose two hypotheses:

Gradient oscillation may contribute to early optimization difficulty. Looped Transformer repeatedly applies the same Transformer backbone across loop iterations, making its training dynamics similar to those of recurrent models optimized through BPTT algorithm [Werbos, 2002]. Although the number of loop iterations is much smaller than the number of time steps in conventional long-sequence RNNs, gradients can still accumulate through the shared looped blocks. We therefore hypothesize that this loop-wise gradient accumulation is one possible source of early gradient oscillation, which makes optimization more sensitive and increases the likelihood of entering unstable training regimes.

Residual explosion may become a bottleneck in highly looped settings. Looping a fixed-depth backbone increases the effective recurrent depth of the computation graph, meaning that unrolling the looped model during training makes it equivalent to a much deeper model on the computation graph. Under this view, even a mild amplification of residual states at each loop iteration can accumulate across repeated applications of the same shared layers. We therefore hypothesize that highly looped LT can develop residual amplification in the recurrent dimension, resulting in residual explosion. Since this phenomenon persists beyond the initial transient, we treat it as a separate instability pattern that may not fully explain early collapse by itself, but can become a major optimization bottleneck when the loop count is large.

Overall, the early diagnostic results reveal two instability patterns in LT training: gradient oscillation during the early optimization phase and residual explosion at high loop counts. These observations motivate the design choices introduced in the next section, where we aim to stabilize looped training without adding learnable parameters.

4 Fully Looped Transformer

In Section 3, we identified two patterns associated with Looped Transformer’s (LT) training instability: gradient oscillation and residual explosion. We design Fully Looped Transformer (FLT) to mitigate these two problems. FLT introduces two improvements: (1) Fully Looped Architecture (FLA) and (2) Attention Injection (AI). Figure 1 shows a comparison of the overall architectures between FLT and LT, as well as the specific implementations of FLA and AI in FLT.

4.1 Fully Looped Architecture

Although all of our models already incorporate RMSNorm [Zhang and Sennrich, 2019] in each layer to regulate the output residual states, residual explosion still occurs. This suggests that normalization alone is insufficient, and that the issue must be addressed from a deeper structural perspective.

In Section 3, we suggest that residual explosion may be due to a large effective recurrent depth of the model, which poses similar optimization challenges as extremely deep neural networks. Extremely deep neural networks require shortcut connections like residual connections [He et al., 2016] to alleviate their optimization difficulties. Veit et al. [2016] indicate that residual connections can help optimize deep models because they are equivalent to reducing the depth of the model during the optimization process. Inspired by these studies, we aim to design a residual connections that works in the recurrent dimension to mitigate the optimization difficulties related to effective recurrent depth.

We propose **Fully Looped Architecture (FLA)** as a recurrent connectivity pattern. In vanilla Looped Transformer, the output of the previous loop iteration is passed only to the first layer of the next iteration. As a result, layers at larger depth can access the recurrent state only through a long chain of intermediate transformations. FLA changes this by making the previous loop output available to every layer in the current iteration. Formally, let $h_L^{(t-1)}$ denote the output hidden state of the previous loop iteration. For each layer l in the current iteration t , FLA defines the layer update as:

$$\mathbf{h}_l^{(t)} = f_\theta^{(l)}\left(\mathbf{h}_{l-1}^{(t)}, \mathbf{h}_L^{(t-1)}\right), \quad l = 1, \dots, L, \quad (1)$$

Here, $f_\theta^{(l)}$ denotes the l -th Transformer layer equipped with a fusion operation that incorporates $h_L^{(t-1)}$. FLA itself only specifies the recurrent connectivity; it does not prescribe how the previous loop state should be fused into each layer. In our ablations, we consider a direct residual-addition implementation, denoted FLT_{res} . In the complete Fully Looped Transformer, we implement this fusion using Attention Injection, which is described in the next subsection.

4.2 Attention Injection

In Section 3, we observed abnormal gradient dynamics during the early stage of pretraining. These dynamics are consistent with the difficulty of RNNs trained with the BPTT algorithm. Gradient clipping [Pascanu et al., 2013] is a common practical mitigation, but it operates as an optimization-level intervention and introduces an additional threshold hyperparameter. Here, we instead explore an architectural mechanism that controls the recurrent signal.

LSTM [Hochreiter and Schmidhuber, 1997] and GRU [Cho et al., 2014] mitigate the gradient explosion problem through gating mechanisms. A key role of these gates is to modulate the information in residual flow within a bounded range, which helps control the magnitude of propagated signals and gradients. Inspired by this principle, we propose **Attention Injection (AI)**, which reuses the Self-Attention module as a Cross-Attention module to inject the previous loop iteration’s hidden state into the current loop step. Instead of adding $h_L^{(t-1)}$ directly into the residual flow, AI uses it as the query of an attention operation. The current layer representation provides the keys and values. In this way, the previous loop state determines which information to retrieve, but the injected activation is constructed from the current value vectors rather than copied directly from the previous residual state.

By routing $\mathbf{h}_L^{(t-1)}$ as the query Q , AI can be viewed as using Softmax operations to control and select information from the residual flow. When $h_L^{(t-1)}$ is used as the query, it influences the injected signal indirectly through attention blocks rather than being directly added to the residual flow. Because the attention weights are normalized by the softmax operation, the injected signal is a normalized mixture of the value vectors. Therefore, the magnitude of the injected recurrent signal is mediated by the current value stream rather than being directly determined by $h_L^{(t-1)}$. This provides a controlled mixing mechanism for recurrent information and reduces the risk of directly amplifying the residual flow. Formally, the standard attention operation is:

$$\text{Attention}(Q, K, V) = \text{Softmax}\left(\frac{QK^\top}{\sqrt{d_k}}\right)V, \quad (2)$$

Concretely, during the first loop iteration ($t = 1$), the model performs standard Self-Attention. In subsequent loop iterations ($t > 1$), the model switches to Cross-Attention: the hidden state from the previous loop iteration $\mathbf{h}_L^{(t-1)}$ is used as the query (Q), while the output of the preceding module $\mathbf{z}_l^{(t)}$ serves as both the key (K) and value (V). Formally, the attention block for $t > 1$ is modified as:

$$\mathbf{a}_l^{(t)} = \text{Attention} \left(Q = W_Q h_L^{(t-1)}, K = W_K z_l^{(t)}, V = W_V z_l^{(t)} \right), \quad (3)$$

where $\mathbf{a}_l^{(t)}$ denotes the output of the attention block at layer l in loop iteration t . In this design, the previous residual state is not directly added into the residual flow. Instead, it acts as a query that selects and reuses information from the current layer representation.

Inspired by Input Injection [Anil et al., 2022], in the first layer of the model, AI directly uses the input embedding \mathbf{x} as the $z_l^{(t)}$. Input Injection adds the input embedding \mathbf{x} to the residual flow at each loop iteration as a method of emphasizing the input signal. Input Injection has been used as an empirical stabilization technique in prior looped models [Zhu et al., 2025]. In our architecture, we hypothesize that first-layer Attention Injection serves a role analogous to Input Injection by reinforcing the input signal through the attention mechanism.

AI reuses the Self-Attention projection matrices W_Q, W_K, W_V as Cross-Attention projection matrices. No additional Cross-Attention parameters, gates, or normalization layers are introduced. We deliberately inject the recurrent signal through Q rather than K or V . This design keeps the key-value streams in the same form as standard attention, preserving compatibility with existing KV-cache reuse mechanisms during loop iteration.

4.3 Implementation Details

In this work, We use the pretrained tokenizer of Qwen3 [Yang et al., 2025] throughout training. We used the μP [Yang et al., 2022] method to adjust the learning rate of models with different depths and optimized the models using the Muon [Jordan et al., 2024b] and AdamW [Loshchilov and Hutter, 2019] optimizers. A fixed batch size was used for all models, and the total number of training tokens was scaled according to the Chinchilla scaling law [Hoffmann et al., 2022] to control the total number of training steps. When comparing two models with an equal number of parameters, we use exactly the same hyperparameters. Following Geiping et al. [2025], we use the standard next-token prediction loss, supervising only the last step. Our Transformer backbone network references the implementation of Karpathy [2025]. For more implementation details, please refer to the Appendix A.2 and A.3.

5 Experiments

5.1 Experimental Setup

Dataset. We used FineWeb-Edu [Lozhkov et al., 2024] as our pretraining dataset and validation dataset. FineWeb-Edu is a widely used high-quality pretraining dataset containing 200B of high-value tokens. The dataset itself has already been deduplicated and refined. Following the Chinchilla scaling law [Hoffmann et al., 2022], we scaled the number of training tokens used proportionally to the total number of model parameters, using 20 tokens per parameter.

Evaluation. In Table 1 and Figure 5, we present the perplexity (PPL) on Wikitext2 [Merity et al., 2016], bits per byte (BPB) on the validation dataset, Core Metric and accuracy on the commonsense reasoning benchmarks for models with different parameter counts and loop iterations. PPL and BPB are two metrics that are commonly used to measure language modeling performance. Core Metric, proposed by DCLM [Li et al., 2024], integrates 21 different evaluation metrics that can be used to evaluate the performance of language models during the pretraining stage. More details and specific benchmark citations provided in Appendix A.4.

Baseline. In the Loop Scaling Experiments, we compare the Fully Looped Transformer (FLT) against three baselines: (1) the original Looped Transformer (LT); (2) the Looped Transformer with Input Injection (LT_i); and (3) the Looped Transformer with Attention Injection applied only at the first layer (LT_{ai}). All baselines are trained at two scales: the **small** size (127M parameters, 6 layers) and the **base** size (318M parameters, 12 layers). When the parameter counts and loop iterations are the same, all models use the same amount of computation during pretraining.

Model	Size	Loop	Wiki2 _{ppl} ↓	Val _{bpb} ↓	Core ↑	LMB ↑	PIQA ↑	Hella ↑	OPQA ↑	ARC-E ↑	ARC-C ↑	Avg. ↑
LT	Small	3	67.80	1.054	8.13	18.70	59.46	27.66	27.00	38.97	23.63	32.57
		6	73.04	1.067	7.20	16.33	57.56	26.79	28.20	36.65	23.29	31.47
		9	78.79	1.115	4.67	12.32	56.90	26.00	26.80	36.48	22.86	30.22
	Base	3	43.12	0.905	16.13	30.07	64.25	35.43	34.60	51.64	27.13	40.52
		6	51.38	0.947	11.43	26.37	61.31	31.36	32.80	43.22	24.31	36.56
		9	-	-	-	-	-	-	-	-	-	-
LT _i	Small	3	62.76	1.043	6.99	20.04	59.63	27.80	27.20	39.56	22.44	32.77
		6	62.53	1.042	7.33	20.39	59.24	27.71	29.39	39.94	23.46	33.35
		9	62.31	1.044	8.38	20.58	58.65	27.76	28.00	38.84	24.23	33.01
	Base	3	40.46	0.900	15.36	31.12	64.68	35.79	33.20	56.06	28.41	41.54
		6	39.58	0.900	15.30	29.92	64.63	36.33	31.40	52.65	26.27	40.20
		9	43.43	0.901	14.72	30.56	64.85	36.24	32.80	53.78	27.81	41.00
LT _{ai}	Small	3	66.11	1.046	7.17	19.75	58.86	27.50	28.20	39.60	23.54	32.90
		6	-	-	-	-	-	-	-	-	-	-
		9	73.59	1.047	6.47	19.65	59.84	27.56	28.20	39.68	24.65	33.26
	Base	3	41.63	0.901	14.10	29.53	62.94	35.81	32.40	51.97	27.64	40.04
		6	41.49	0.899	14.97	30.35	62.89	36.33	34.00	52.81	26.62	40.05
		9	42.43	0.901	13.74	28.39	64.41	35.94	32.00	50.96	28.07	39.96
FLT	Small	3	62.76	1.044	5.72	18.39	59.14	27.48	25.80	39.56	22.44	32.13
		6	60.07	1.039	6.34	19.25	58.97	27.91	27.80	37.45	23.03	32.40
		9	63.29	1.040	6.94	19.03	59.14	28.20	25.60	38.88	23.89	32.45
	Base	3	40.47	0.898	15.37	30.64	63.81	35.72	31.80	51.09	26.36	39.90
		6	39.51	0.892	15.60	31.15	64.85	37.03	35.20	52.81	27.24	41.38
		9	38.44	0.892	16.16	32.75	65.07	37.05	33.20	53.87	28.41	41.72

Table 1: Comparison of different loop language model variants across Small and Base sizes on language modeling metrics and downstream tasks. Avg. is the unweighted average of LAMBADA OpenAI (LMB), PIQA, HellaSwag (Hella.), Openbook QA (OPQA), ARC-Easy (ARC-E) and ARC-Challenge (ARC-C). Core Metrics, Wiki2 PPL, and validation BPB are not included. "-" indicates that model collapsed; therefore it was not evaluated. Bold text indicates the best value for each metric.

Ablation. In the ablation experiment, We check the stability of different methods using the same settings as Section 3. In addition to the baselines mentioned above, we also compared the Fully Looped Transformer variant (FLT_{res}), which implements the Fully Looped Architecture by directly adding the hidden state to the residual flow instead of using Attention Injection. This variant exhibited training collapse under various looping settings, therefore, we do not directly compare it with other architectures in the loop scaling experiment, but instead to compare the characteristics of different architectures in the ablation experiment. By default, we implement Attention Injection with Full Attention (FA) [Vaswani et al., 2023]. We also experimented to see if Attention Injection could be applied to different attention mechanism variants, including Sliding Window Attention (SWA) [Beltagy et al., 2020], Multi-head Latent Attention (MLA) [DeepSeek-AI et al., 2024] and Grouped-Query Attention (GQA) [Ainslie et al., 2023]. Please refer to Appendix A.2 and A.3 for more experiment and training setup details.

5.2 Loop Scaling Experiments

As shown in Table 1, the original LT degrades as the number of loop iterations increases. At the small size, its downstream-task average drops from 32.57 to 30.22, while Wiki2 PPL, validation BPB, and the Core Metric also worsen. LT_i and FLT are more stable, with LT_i obtaining the best small-size average of 33.35 at 6 loops; LT_{ai} fails to converge in this setting. FLT trains stably across all loop settings and improves from 32.13 to 32.45. These results suggest that the modified variants are less sensitive to increased loop depth than the original LT.

At the base size, the advantage of FLT is clearer. The original LT drops from 40.52 to 36.56 between 3 and 6 loops and collapses at 9 loops, while LT_i and LT_{ai} show only fluctuating or saturated gains. FLT is the only variant whose downstream-task average consistently increases, reaching 41.72 at 9 loops, where it also achieves the best average score, the lowest Wiki2 PPL, the highest Core Metric, and a tied-best validation BPB. This indicates that FLT benefits more reliably from additional loop iterations when model size increases.

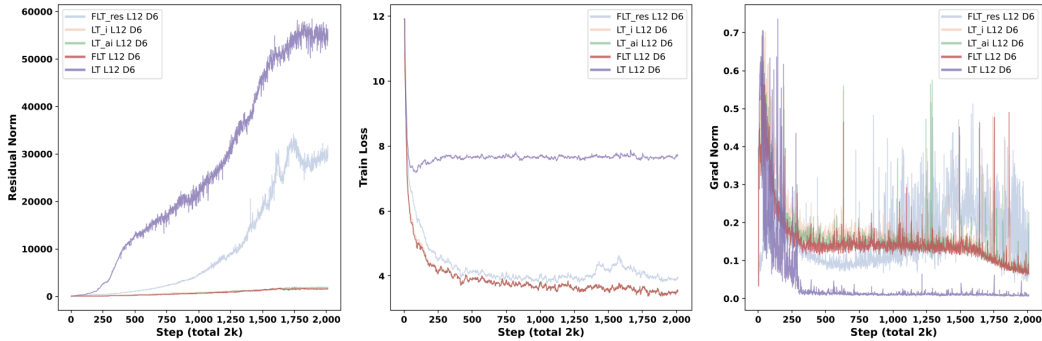


Figure 3: Training dynamics comparison of the FLT variants and LT variants. All models compared in the same graph use the same number of parameters and loop iterations. **Left**: comparison chart of residual-state norms in the first loop iteration. **Middle**: comparison chart of training loss. Curves are smoothed with an exponential moving average coefficient of 0.9 for readability. **Right**: comparison chart of the gradient L2 norm of the first FFN block.

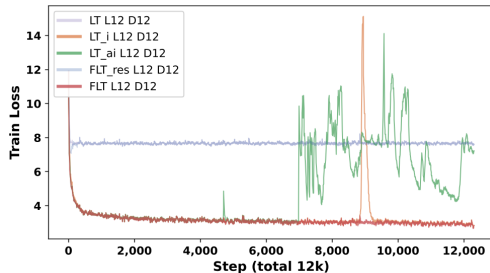


Figure 4: The loss of different base size models at 12-loop setting. All models except FLT collapsed. Smoothed with factor 0.9 for readability.

Metrics	GQA	MLA	SWA	FA
Wiki2 _{ppl} ↓	39.68	38.76	38.91	41.12
Val _{bbp} ↓	0.897	0.904	0.895	0.895
Core ↑	16.24	15.64	15.58	15.66

Table 2: Pretraining performance metrics of four Base-size FLT models with 12 loop iterations, where Attention Injection is implemented with different attention mechanism variants. All four models stably completed training and achieved high evaluation performance.

Overall, FLT provides the most stable scaling behavior with increasing loop iterations. At the base size, its Wiki2 PPL decreases from 40.47 to 38.44, its Core Metric rises from 15.37 to 16.16, and its validation BPB improves from 0.898 to 0.892. Although LT_i remains competitive at the small size, FLT achieves the strongest base-size result. In particular, at 6 loops, FLT outperforms the original LT by 4.82 absolute points, corresponding to a relative improvement of about 13.2%. These findings show that FLT offers a better balance between downstream performance and training stability.

5.3 Ablation Experiments

In this section, we conducted a comprehensive set of ablation experiments to observe and verify whether our two proposed improvements effectively improve training stability. The ablation experiment results are presented in Figure 3, from which we draw the following four conclusions.

Fully Looped Architecture attenuates residual explosion. Although FLT_{res} still exhibits residual explosion, its residuals are significantly smaller than those of the original LT. Meanwhile, the Fully Looped Architecture implemented using Attention Injection performs even better, with no residual explosion observed throughout the training process. This indicates that FLA attenuates residual amplification, but is not sufficient by itself to guarantee stable training.

Attention Injection can take on the role of Input Injection. Applying Attention Injection only at the first layer yields behavior comparable to Input Injection in several settings. This implies that the role of Input Injection primarily lie in aggregating the input with the looping residual state, a function that Attention Injection naturally fulfills through attention mechanism. However, first-layer Attention Injection alone is not sufficient to guarantee stability in highly looped settings, as shown by the collapse cases in Table 1 and Figure 4. The first-layer Attention Injection indeed serves a role analogous to Input Injection through the attention mechanism.

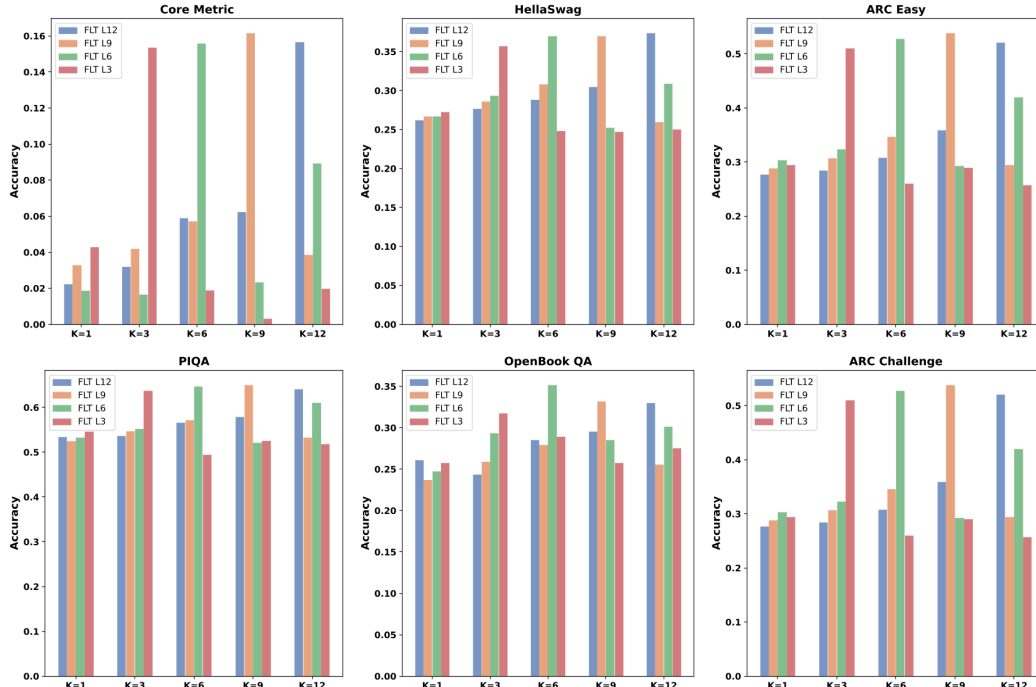


Figure 5: Test-time adaptation evaluation results of FLT. Models trained with 3, 6, 9, or 12 loop iterations are evaluated using 1, 3, 6, 9, and 12 loop iterations. The y-axis reports accuracy.

Attention Injection can be applied with various attention mechanisms. As shown in Table 2, FLT trained with different attention mechanisms can complete training stably and achieve performance comparable to Full Attention, with 12 loop iterations at the base size. This result demonstrates that Attention Injection is robust and compatible. More experimental results are provided in Appendix A.1.2.

The combination of Fully Looped Architecture and Attention Injection performs best. Figure 4 shows that Input Injection or first-layer Attention Injection alone can still be unstable in the 12-loop setting. Under the same setup, Figure 3 (middle and right) shows that applying the Fully Looped Architecture alone leads to gradient oscillation and training collapse.

5.4 Test-Time Compute Adaptation Experiments

In this section, we try to answer the following question: after training with a fixed number of loop iterations, can Fully Looped Transformer still adapt to different numbers of loop iterations during inference? For models pretrained with 3, 6, 9, and 12 loop iterations, we evaluated their performance at 1, 3, 6, 9, and 12 loop iterations, as shown in Figure 5. When the loop count at inference exceeds the maximum used during pretraining, performance begins to fluctuate, indicating that the model struggles to adapt to excessive computational resources. However, when it stays within the pretraining range, highly looped models such as those with 9 or 12 loop iterations show a positive correlation between performance and the number of loop iterations, meaning that more computational resources lead to better performance. These results provide preliminary evidence that FLT can exploit additional test-time loop iterations within the range seen during training. However, performance becomes less predictable when the inference loop count exceeds the training loop count, suggesting that explicit training over variable loop counts may be necessary for robust test-time compute adaptation.

6 Limitation

Our study is limited to the model scales and architectures evaluated in this work; whether Fully Looped Transformer remains effective for deeper backbones, larger models, and more diverse settings requires further validation. Due to the cost of pretraining multiple looped language models, we use a single run per configuration and do not report training-run error bars. Future work should examine residual-state supervision, interpretability, and robustness across random seeds and larger scales.

7 Conclusion

In this work, we systematically investigate the training instability of the Looped Transformer and identify gradient oscillation and residual explosion as two key phenomena associated with this problem. To this end, we propose the Fully Looped Transformer, a simple parameter-free improvement over the naive Looped Transformer that stabilizes inter-loop information propagation and suppresses gradient oscillation through Fully Looped Architecture and Attention Injection. Our model improves training stability and downstream-task performance without increasing the parameter count, remains compatible with common attention variants, and offers preliminary adaptability by adjusting loop iterations at inference. We hope our findings deepen the understanding of Looped Transformer training dynamics and inspire future stable, parameter-efficient, and adaptive architectures.

References

- J. Ainslie, J. Lee-Thorp, M. de Jong, Y. Zemlyanskiy, F. Lebrón, and S. Sanghai. Gqa: Training generalized multi-query transformer models from multi-head checkpoints, 2023. URL <https://arxiv.org/abs/2305.13245>.
- C. Anil, A. Pople, K. Liang, J. Treutlein, Y. Wu, S. Bai, J. Z. Kolter, and R. B. Grosse. Path independent equilibrium models can better exploit test-time computation. *Advances in Neural Information Processing Systems*, 35:7796–7809, 2022.
- I. Beltagy, M. E. Peters, and A. Cohan. Longformer: The long-document transformer, 2020. URL <https://arxiv.org/abs/2004.05150>.
- Y. Bengio, P. Simard, and P. Frasconi. Learning long-term dependencies with gradient descent is difficult. *IEEE transactions on neural networks*, 5(2):157–166, 1994.
- Y. Bisk, R. Zellers, R. L. Bras, J. Gao, and Y. Choi. Piqa: Reasoning about physical commonsense in natural language. In *Thirty-Fourth AAAI Conference on Artificial Intelligence*, 2020.
- K. Cho, B. Van Merriënboer, Ç. Gulçehre, D. Bahdanau, F. Bougares, H. Schwenk, and Y. Bengio. Learning phrase representations using rnn encoder–decoder for statistical machine translation. In *Proceedings of the 2014 conference on empirical methods in natural language processing (EMNLP)*, pages 1724–1734, 2014.
- P. Clark, I. Cowhey, O. Etzioni, T. Khot, A. Sabharwal, C. Schoenick, and O. Tafjord. Think you have solved question answering? try arc, the ai2 reasoning challenge. *arXiv:1803.05457v1*, 2018.
- DeepSeek-AI, A. Liu, B. Feng, B. Wang, B. Wang, B. Liu, C. Zhao, C. Dengr, C. Ruan, D. Dai, D. Guo, D. Yang, D. Chen, D. Ji, E. Li, F. Lin, F. Luo, G. Hao, G. Chen, G. Li, H. Zhang, H. Xu, H. Yang, H. Zhang, H. Ding, H. Xin, H. Gao, H. Li, H. Qu, J. L. Cai, J. Liang, J. Guo, J. Ni, J. Li, J. Chen, J. Yuan, J. Qiu, J. Song, K. Dong, K. Gao, K. Guan, L. Wang, L. Zhang, L. Xu, L. Xia, L. Zhao, L. Zhang, M. Li, M. Wang, M. Zhang, M. Zhang, M. Tang, M. Li, N. Tian, P. Huang, P. Wang, P. Zhang, Q. Zhu, Q. Chen, Q. Du, R. J. Chen, R. L. Jin, R. Ge, R. Pan, R. Xu, R. Chen, S. S. Li, S. Lu, S. Zhou, S. Chen, S. Wu, S. Ye, S. Ma, S. Wang, S. Zhou, S. Yu, S. Zhou, S. Zheng, T. Wang, T. Pei, T. Yuan, T. Sun, W. L. Xiao, W. Zeng, W. An, W. Liu, W. Liang, W. Gao, W. Zhang, X. Q. Li, X. Jin, X. Wang, X. Bi, X. Liu, X. Wang, X. Shen, X. Chen, X. Chen, X. Nie, X. Sun, X. Wang, X. Liu, X. Xie, X. Yu, X. Song, X. Zhou, X. Yang, X. Lu, X. Su, Y. Wu, Y. K. Li, Y. X. Wei, Y. X. Zhu, Y. Xu, Y. Huang, Y. Li, Y. Zhao, Y. Sun, Y. Li, Y. Wang, Y. Zheng, Y. Zhang, Y. Xiong, Y. Zhao, Y. He, Y. Tang, Y. Piao, Y. Dong, Y. Tan, Y. Liu, Y. Wang, Y. Guo, Y. Zhu, Y. Wang, Y. Zou, Y. Zha, Y. Ma, Y. Yan, Y. You, Y. Liu, Z. Z. Ren, Z. Ren, Z. Sha, Z. Fu, Z. Huang, Z. Zhang, Z. Xie, Z. Hao, Z. Shao, Z. Wen, Z. Xu, Z. Zhang, Z. Li, Z. Wang, Z. Gu, Z. Li, and Z. Xie. Deepseek-v2: A strong, economical, and efficient mixture-of-experts language model, 2024. URL <https://arxiv.org/abs/2405.04434>.
- M. Dehghani, S. Gouws, O. Vinyals, J. Uszkoreit, and L. Kaiser. Universal transformers. In *International Conference on Learning Representations*, 2019.
- J. Geiping, S. McLeish, N. Jain, J. Kirchenbauer, S. Singh, B. R. Bartoldson, B. Kaillkhura, A. Bhatele, and T. Goldstein. Scaling up test-time compute with latent reasoning: A recurrent depth approach. *arXiv preprint arXiv:2502.05171*, 2025.

- A. Giannou, S. Rajput, J.-y. Sohn, K. Lee, J. D. Lee, and D. Papailiopoulos. Looped transformers as programmable computers. In *International Conference on Machine Learning*, pages 11398–11442. PMLR, 2023.
- D. Guo, D. Yang, H. Zhang, J. Song, P. Wang, Q. Zhu, R. Xu, R. Zhang, S. Ma, X. Bi, et al. Deepseek-r1: Incentivizing reasoning capability in llms via reinforcement learning. *arXiv preprint arXiv:2501.12948*, 2025.
- K. He, X. Zhang, S. Ren, and J. Sun. Deep residual learning for image recognition. In *Proceedings of the IEEE conference on computer vision and pattern recognition*, pages 770–778, 2016.
- A. Henry, P. R. Dachapally, S. Pawar, and Y. Chen. Query-key normalization for transformers, 2020. URL <https://arxiv.org/abs/2010.04245>.
- S. Hochreiter and J. Schmidhuber. Long short-term memory. *Neural computation*, 9(8):1735–1780, 1997.
- J. Hoffmann, S. Borgeaud, A. Mensch, E. Buchatskaya, T. Cai, E. Rutherford, D. Casas, L. A. Hendricks, J. Welbl, A. Clark, et al. Training compute-optimal large language models. *arXiv preprint arXiv:2203.15556*, 10, 2022.
- K. Jordan, J. Bernstein, B. Rappazzo, @fernbear.bsky.social, B. Vlado, Y. Jiacheng, F. Cesista, B. Koszarsky, and @Grad62304977. modded-nanogpt: Speedrunning the nanogpt baseline, 2024a. URL <https://github.com/KellerJordan/modded-nanogpt>.
- K. Jordan, Y. Jin, V. Boza, J. You, F. Cesista, L. Newhouse, and J. Bernstein. Muon: An optimizer for hidden layers in neural networks, 2024b. URL <https://kellerjordan.github.io/posts/muon/>.
- A. Karpathy. nanochat: The best chatgpt that \$100 can buy, 2025. URL <https://github.com/karpathy/nanochat>.
- Y. Koisshenkov, A. Lipani, and N. Cancedda. Encode, think, decode: Scaling test-time reasoning with recursive latent thoughts. *arXiv preprint arXiv:2510.07358*, 2025.
- J. Li, A. Fang, G. Smyrnis, M. Ivgi, M. Jordan, S. Gadre, H. Bansal, E. Guha, S. Keh, K. Arora, et al. Datacomp-lm: In search of the next generation of training sets for language models. *Advances in Neural Information Processing Systems*, 37:14200–14282, 2024.
- I. Loshchilov and F. Hutter. Decoupled weight decay regularization, 2019. URL <https://arxiv.org/abs/1711.05101>.
- A. Lozhkov, L. Ben Allal, L. von Werra, and T. Wolf. Fineweb-edu: the finest collection of educational content, 2024. URL <https://huggingface.co/datasets/HuggingFaceFW/fineweb-edu>.
- S. Merity, C. Xiong, J. Bradbury, and R. Socher. Pointer sentinel mixture models, 2016.
- T. Mihaylov, P. Clark, T. Khot, and A. Sabharwal. Can a suit of armor conduct electricity? a new dataset for open book question answering. In *EMNLP*, 2018.
- J. Niklaus, G. Penedo, H. Kydlicek, E. Bakouch, L. Tunstall, E. Beeching, T. Frere, C. Raffel, L. von Werra, and T. Wolf. The synthetic data playbook: Generating trillions of the finest tokens, 2026.
- D. Paperno, G. Kruszewski, A. Lazaridou, Q. N. Pham, R. Bernardi, S. Pezzelle, M. Baroni, G. Boleda, and R. Fernández. The lambda dataset: Word prediction requiring a broad discourse context, 2016. URL <https://arxiv.org/abs/1606.06031>.
- R. Pascanu, T. Mikolov, and Y. Bengio. On the difficulty of training recurrent neural networks. In *International conference on machine learning*, pages 1310–1318. Pmlr, 2013.
- H. Prairie, Z. Novack, T. Berg-Kirkpatrick, and D. Y. Fu. Parcae: Scaling laws for stable looped language models. *arXiv preprint arXiv:2604.12946*, 2026.
- A. Radford, J. Wu, R. Child, D. Luan, D. Amodei, and I. Sutskever. Language models are unsupervised multitask learners. 2019.

- S. Rajbhandari, J. Rasley, O. Ruwase, and Y. He. Zero: Memory optimizations toward training trillion parameter models, 2020. URL <https://arxiv.org/abs/1910.02054>.
- N. Saunshi, N. Dikkala, Z. Li, S. Kumar, and S. J. Reddi. Reasoning with latent thoughts: On the power of looped transformers. *arXiv preprint arXiv:2502.17416*, 2025.
- J. Su, Y. Lu, S. Pan, A. Murtadha, B. Wen, and Y. Liu. Roformer: Enhanced transformer with rotary position embedding, 2023. URL <https://arxiv.org/abs/2104.09864>.
- G. Team, M. Riviere, S. Pathak, P. G. Sessa, C. Hardin, S. Bhupatiraju, L. Hussenot, T. Mesnard, B. Shahriari, A. Ramé, J. Ferret, P. Liu, P. Tafti, A. Friesen, M. Casbon, S. Ramos, R. Kumar, C. L. Lan, S. Jerome, A. Tsitsulin, N. Vieillard, P. Stanczyk, S. Girgin, N. Momchev, M. Hoffman, S. Thakoor, J.-B. Grill, B. Neyshabur, O. Bachem, A. Walton, A. Severyn, A. Parrish, A. Ahmad, A. Hutchison, A. Abdagic, A. Carl, A. Shen, A. Brock, A. Coenen, A. Laforge, A. Paterson, B. Bastian, B. Piot, B. Wu, B. Royal, C. Chen, C. Kumar, C. Perry, C. Welty, C. A. Choquette-Choo, D. Sinopalnikov, D. Weinberger, D. Vijaykumar, D. Rogozińska, D. Herbison, E. Bandy, E. Wang, E. Noland, E. Moreira, E. Senter, E. Eltyshv, F. Visin, G. Rasskin, G. Wei, G. Cameron, G. Martins, H. Hashemi, H. Klimczak-Plucińska, H. Batra, H. Dhand, I. Nardini, J. Mein, J. Zhou, J. Svensson, J. Stanway, J. Chan, J. P. Zhou, J. Carrasqueira, J. Iljazi, J. Becker, J. Fernandez, J. van Amersfoort, J. Gordon, J. Lipschultz, J. Newlan, J. yeong Ji, K. Mohamed, K. Badola, K. Black, K. Millican, K. McDonell, K. Nguyen, K. Sodhia, K. Greene, L. L. Sjoesund, L. Usui, L. Sifre, L. Heuermann, L. Lago, L. McNealus, L. B. Soares, L. Kilpatrick, L. Dixon, L. Martins, M. Reid, M. Singh, M. Iverson, M. Görner, M. Velloso, M. Wirth, M. Davidow, M. Miller, M. Rahtz, M. Watson, M. Risdal, M. Kazemi, M. Moynihan, M. Zhang, M. Kahng, M. Park, M. Rahman, M. Khatwani, N. Dao, N. Bardoliwalla, N. Devanathan, N. Dumai, N. Chauhan, O. Wahltinez, P. Botarda, P. Barnes, P. Barham, P. Michel, P. Jin, P. Georgiev, P. Culliton, P. Kuppala, R. Comanescu, R. Merhej, R. Jana, R. A. Rokni, R. Agarwal, R. Mullins, S. Saadat, S. M. Carthy, S. Cogan, S. Perrin, S. M. R. Arnold, S. Krause, S. Dai, S. Garg, S. Sheth, S. Ronstrom, S. Chan, T. Jordan, T. Yu, T. Eccles, T. Hennigan, T. Kocisky, T. Doshi, V. Jain, V. Yadav, V. Meshram, V. Dharmadhikari, W. Barkley, W. Wei, W. Ye, W. Han, W. Kwon, X. Xu, Z. Shen, Z. Gong, Z. Wei, V. Cotruta, P. Kirk, A. Rao, M. Giang, L. Peran, T. Warkentin, E. Collins, J. Barral, Z. Ghahramani, R. Hadsell, D. Sculley, J. Banks, A. Dragan, S. Petrov, O. Vinyals, J. Dean, D. Hassabis, K. Kavukcuoglu, C. Farabet, E. Buchatskaya, S. Borgeaud, N. Fiedel, A. Joulin, K. Kenealy, R. Dadashi, and A. Andreev. Gemma 2: Improving open language models at a practical size, 2024. URL <https://arxiv.org/abs/2408.00118>.
- O. team, A. Jaech, A. Kalai, A. Lerer, A. Richardson, A. El-Kishky, A. Low, A. Helyar, A. Madry, A. Beutel, A. Carney, A. Iftimie, A. Karpenko, A. T. Passos, A. Neitz, A. Prokofiev, A. Wei, A. Tam, A. Bennett, A. Kumar, A. Saraiva, A. Vallone, A. Duberstein, A. Kondrich, A. Mishchenko, A. Applebaum, A. Jiang, A. Nair, B. Zoph, B. Ghorbani, B. Rossen, B. Sokolowsky, B. Barak, B. McGrew, B. Minaiev, B. Hao, B. Baker, B. Houghton, B. McKinzie, B. Eastman, C. Lugaresi, C. Bassin, C. Hudson, C. M. Li, C. de Bourcy, C. Voss, C. Shen, C. Zhang, C. Koch, C. Orsinger, C. Hesse, C. Fischer, C. Chan, D. Roberts, D. Kappler, D. Levy, D. Selsam, D. Dohan, D. Farhi, D. Mely, D. Robinson, D. Tsipras, D. Li, D. Oprica, E. Freeman, E. Zhang, E. Wong, E. Proehl, E. Cheung, E. Mitchell, E. Wallace, E. Ritter, E. Mays, F. Wang, F. P. Such, F. Raso, F. Leoni, F. Tsimpourlas, F. Song, F. von Lohmann, F. Sulit, G. Salmon, G. Parascandolo, G. Chabot, G. Zhao, G. Brockman, G. Leclerc, H. Salman, H. Bao, H. Sheng, H. Andrin, H. Bagherinezhad, H. Ren, H. Lightman, H. W. Chung, I. Kivlichan, I. O’Connell, I. Osband, I. C. Gilaberte, I. Akkaya, I. Kostrikov, I. Sutskever, I. Kofman, J. Pachocki, J. Lennon, J. Wei, J. Harb, J. Twore, J. Feng, J. Yu, J. Weng, J. Tang, J. Yu, J. Q. Candela, J. Palermo, J. Parish, J. Heidecke, J. Hallman, J. Rizzo, J. Gordon, J. Uesato, J. Ward, J. Huizinga, J. Wang, K. Chen, K. Xiao, K. Singhal, K. Nguyen, K. Cobbe, K. Shi, K. Wood, K. Rimbach, K. Gu-Lemberg, K. Liu, K. Lu, K. Stone, K. Yu, L. Ahmad, L. Yang, L. Liu, L. Maksin, L. Ho, L. Fedus, L. Weng, L. Li, L. McCallum, L. Held, L. Kuhn, L. Kondraciuk, L. Kaiser, L. Metz, M. Boyd, M. Trebacz, M. Joglekar, M. Chen, M. Tintor, M. Meyer, M. Jones, M. Kaufer, M. Schwarzer, M. Shah, M. Yatbaz, M. Y. Guan, M. Xu, M. Yan, M. Glaese, M. Chen, M. Lampe, M. Malek, M. Wang, M. Fradin, M. McClay, M. Pavlov, M. Wang, M. Wang, M. Murati, M. Bavarian, M. Rohaninejad, N. McAleese, N. Chowdhury, N. Chowdhury, N. Ryder, N. Tezak, N. Brown, O. Nachum, O. Boiko, O. Murk, O. Watkins, P. Chao, P. Ashbourne, P. Izmailov, P. Zhokhov, R. Dias, R. Arora, R. Lin, R. G. Lopes, R. Gaon, R. Miyara, R. Leike, R. Hwang, R. Garg, R. Brown, R. James, R. Shu, R. Cheu, R. Greene, S. Jain, S. Altman, S. Toizer,

- S. Toyer, S. Miserendino, S. Agarwal, S. Hernandez, S. Baker, S. McKinney, S. Yan, S. Zhao, S. Hu, S. Santurkar, S. R. Chaudhuri, S. Zhang, S. Fu, S. Papay, S. Lin, S. Balaji, S. Sanjeev, S. Sidor, T. Broda, A. Clark, T. Wang, T. Gordon, T. Sanders, T. Patwardhan, T. Sottiaux, T. Degry, T. Dimson, T. Zheng, T. Garipov, T. Stasi, T. Bansal, T. Creech, T. Peterson, T. Eloundou, V. Qi, V. Kosaraju, V. Monaco, V. Pong, V. Fomenko, W. Zheng, W. Zhou, W. McCabe, W. Zaremba, Y. Dubois, Y. Lu, Y. Chen, Y. Cha, Y. Bai, Y. He, Y. Zhang, Y. Wang, Z. Shao, and Z. Li. Openai o1 system card, 2024. URL <https://arxiv.org/abs/2412.16720>.
- A. Vaswani, N. Shazeer, N. Parmar, J. Uszkoreit, L. Jones, A. N. Gomez, L. Kaiser, and I. Polosukhin. Attention is all you need, 2023. URL <https://arxiv.org/abs/1706.03762>.
- A. Veit, M. Wilber, and S. Belongie. Residual networks behave like ensembles of relatively shallow networks, 2016. URL <https://arxiv.org/abs/1605.06431>.
- P. Villalobos, A. Ho, J. Sevilla, T. Besiroglu, L. Heim, and M. Hobbhahn. Position: Will we run out of data? limits of llm scaling based on human-generated data. In *Forty-first International Conference on Machine Learning*, 2024.
- J. Wei, X. Wang, D. Schuurmans, M. Bosma, B. Ichter, F. Xia, E. Chi, Q. Le, and D. Zhou. Chain-of-thought prompting elicits reasoning in large language models, 2023. URL <https://arxiv.org/abs/2201.11903>.
- P. J. Werbos. Backpropagation through time: what it does and how to do it. *Proceedings of the IEEE*, 78(10):1550–1560, 2002.
- A. Yang, A. Li, B. Yang, B. Zhang, B. Hui, B. Zheng, B. Yu, C. Gao, C. Huang, C. Lv, C. Zheng, D. Liu, F. Zhou, F. Huang, F. Hu, H. Ge, H. Wei, H. Lin, J. Tang, J. Yang, J. Tu, J. Zhang, J. Yang, J. Yang, J. Zhou, J. Zhou, J. Lin, K. Dang, K. Bao, K. Yang, L. Yu, L. Deng, M. Li, M. Xue, M. Li, P. Zhang, P. Wang, Q. Zhu, R. Men, R. Gao, S. Liu, S. Luo, T. Li, T. Tang, W. Yin, X. Ren, X. Wang, X. Zhang, X. Ren, Y. Fan, Y. Su, Y. Zhang, Y. Zhang, Y. Wan, Y. Liu, Z. Wang, Z. Cui, Z. Zhang, Z. Zhou, and Z. Qiu. Qwen3 technical report, 2025. URL <https://arxiv.org/abs/2505.09388>.
- G. Yang, E. J. Hu, I. Babuschkin, S. Sidor, X. Liu, D. Farhi, N. Ryder, J. Pachocki, W. Chen, and J. Gao. Tensor programs v: Tuning large neural networks via zero-shot hyperparameter transfer, 2022. URL <https://arxiv.org/abs/2203.03466>.
- R. Zellers, A. Holtzman, Y. Bisk, A. Farhadi, and Y. Choi. Hellaswag: Can a machine really finish your sentence? In *Proceedings of the 57th Annual Meeting of the Association for Computational Linguistics*, 2019.
- B. Zhang and R. Sennrich. Root mean square layer normalization, 2019. URL <https://arxiv.org/abs/1910.07467>.
- Z. Zhang, Y. Song, G. Yu, X. Han, Y. Lin, C. Xiao, C. Song, Z. Liu, Z. Mi, and M. Sun. Relu² wins: Discovering efficient activation functions for sparse llms, 2024. URL <https://arxiv.org/abs/2402.03804>.
- R.-J. Zhu, Z. Wang, K. Hua, T. Zhang, Z. Li, H. Que, B. Wei, Z. Wen, F. Yin, H. Xing, et al. Scaling latent reasoning via looped language models. *arXiv preprint arXiv:2510.25741*, 2025.

A Appendix

A.1 Additional Experiments Results

A.1.1 Diagnose Experiment

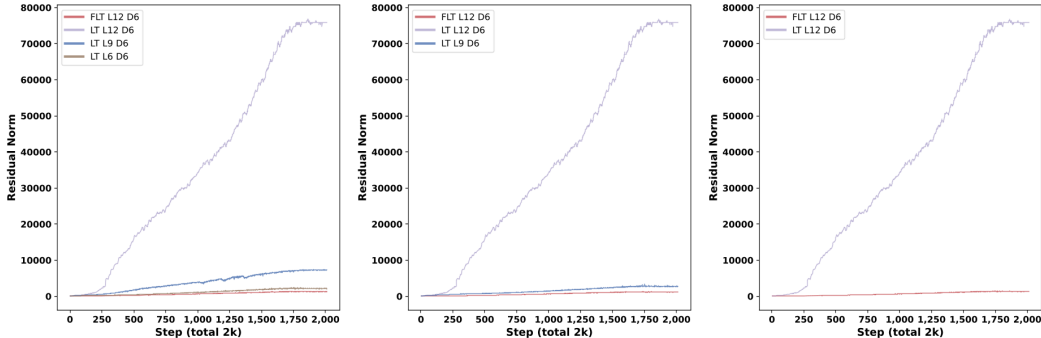


Figure 6: **Left:** the residual norm at the 6th loop iteration. **Middle:** the residual norm at the 9th loop iteration. **Right:** the residual norm at the 12th loop iteration.

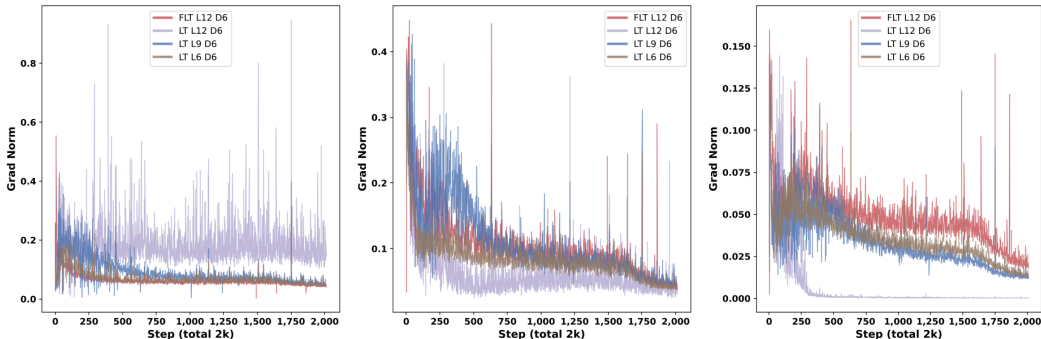


Figure 7: **Left:** the gradient norm of LM head block. **Middle:** the gradient norm of FFN at 5th layer. **Right:** the gradient norm of attention block at 5th layer.

Figures 6 and 7 provide supplementary evidence for the diagnostic experiment in Section 3. Figure 6 extends the residual-state norm analysis to later loop iterations. Compared with the first-loop residual norm shown in the main text, these results show that the residual amplification of vanilla LT becomes more pronounced as the recurrent computation proceeds, especially under larger loop counts. In contrast, FLT keeps the residual-state norms substantially smaller and more stable across loop iterations. This further supports our diagnosis that highly looped LT suffers from residual explosion, while FLT mitigates this instability by stabilizing recurrent information propagation.

Figure 7 reports gradient norms from additional modules, including the LM head, an intermediate FFN block, and an intermediate attention block. These results show that the gradient oscillation observed in the main diagnostic figure is not restricted to the first FFN block, but also appears in other parts of the model during early training. Therefore, Figures 6 and 7 together strengthen the conclusion that LT instability is associated with both residual explosion and gradient oscillation, whereas FLT alleviates both phenomena.

A.1.2 Ablation Experiment

Figures 8 and 9 provide supplementary results for the ablation experiment in Section 5.3. Figure 8 shows the Core Metric trajectories of FLT when Attention Injection is implemented with different attention variants, including Full Attention, Sliding Window Attention, Multi-head Latent Attention, and Grouped-Query Attention. The comparable trends across these variants indicate that the effectiveness of Attention Injection is not tied to a single attention implementation.

Figure 9 further reports the corresponding training-loss curves. All attention variants train stably without collapse, which is consistent with the results in Table 2. These observations support the

conclusion that Attention Injection is compatible with multiple attention mechanisms and can serve as a robust stabilization component for Fully Looped Transformer.

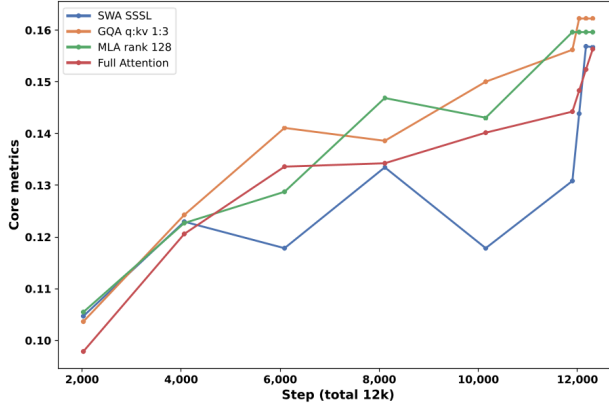


Figure 8: Trend chart of Core Metric changes for FLT with different attention variants throughout the training process

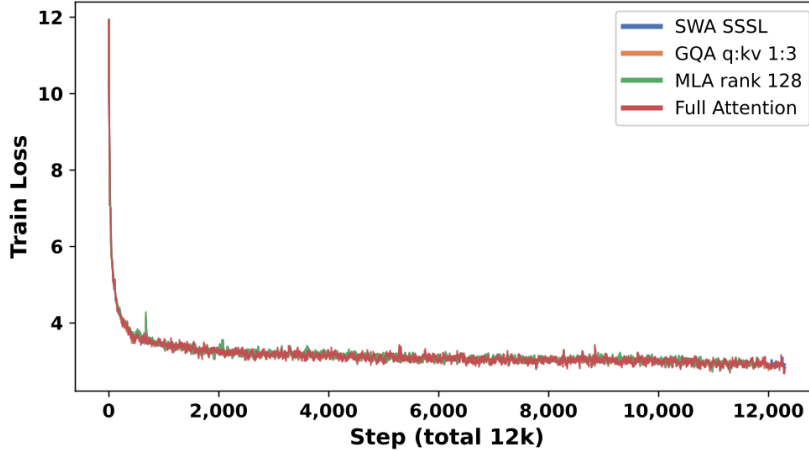


Figure 9: The training loss of FLT with different attention variants. Smoothed with factor 0.9.

A.2 Training Details

Data

We train on a publicly available pretraining corpus streamed from Parquet files and tokenized on-the-fly using a BPE tokenizer with vocabulary size $|\mathcal{V}| = 151643$ (padded to 151644 for divisibility). Data is loaded in a DDP-aware manner: each rank reads disjoint row groups from the Parquet shards. The final Parquet shard is held out as the validation set.

Optimization

We use two optimizers running in parallel, following the approach of modded-nanogpt [Jordan et al., 2024a]:

Muon [Jordan et al., 2024b] for transformer block linear layers. Muon runs standard SGD with momentum internally, then replaces each 2-D parameter update G with the nearest orthogonal matrix via a 5-step Newton–Schulz iteration:

$$X \leftarrow aX + b(XX^\top)X + c(XX^\top)^2X, \quad (a, b, c) = (3.4445, -4.7750, 2.0315). \quad (4)$$

We use learning rate $\eta_{\text{Muon}} = 0.02$ and momentum $\mu = 0.95$ (warmed up from 0.85 over the first 300 steps).

AdamW [Loshchilov and Hutter, 2019] for embeddings and LM head. We use $\beta_1 = 0.8$, $\beta_2 = 0.95$, $\varepsilon = 10^{-10}$, no weight decay. Learning rates are set to $\eta_{\text{embed}} = 0.2$ and $\eta_{\text{head}} = 0.004$, and are scaled by $\sqrt{768/d_{\text{model}}}$ for models with $d_{\text{model}} \neq 768$, following the μP -style depth-scaling convention.

Learning Rate Schedule

We use a trapezoidal schedule with no warm-up: the learning rate is held constant for the first 80% of training, then linearly decayed to zero over the final 20%. All parameters share the same multiplicative schedule factor.

Batch Size and Gradient Accumulation

We use a fixed total batch size of $2^{19} = 524,288$ tokens per optimizer step, with a sequence length of $T = 1024$. When training on N_{GPU} GPUs each processing a per-device batch of B_{dev} sequences, gradient accumulation runs for $\lceil 524,288 / (B_{\text{dev}} \cdot T \cdot N_{\text{GPU}}) \rceil$ micro-steps automatically.

Training Length

Unless otherwise specified, we follow the Chinchilla optimal ratio Hoffmann et al. [2022] and train for a number of steps such that the total token count equals $20 \times N_{\text{params}}$, where N_{params} counts all parameters excluding the token embedding.

Regularization and Precision

We apply gradient clipping with maximum norm 1.0. No dropout or weight decay is used. All forward passes and backward passes use bfloat16 mixed precision (`torch.amp.autocast`); the token embedding is stored in bfloat16 throughout training. `torch.compile` (TorchInductor, `dynamic=False`) is enabled for the training graph.

Distributed Training

We use PyTorch DDP with `torchrun`. The Muon optimizer uses a distributed variant (DistMuon) where Newton–Schulz orthogonalization is computed independently on each rank but momentum buffers are kept in sync. The AdamW optimizer uses ZeRO-2 [Rajbhandari et al., 2020] sharding (DistAdamW) to reduce optimizer state memory. Our models were trained on $8 \times$ A100 GPUs with 80GB RAM with $32 \times$ Intel Xeon CPU processor. At most trained of 5 days for one model.

Diagnostic metrics

For the diagnostic experiments in Section 3, we record the following quantities every evaluation interval. The residual-state norm is computed as the root-mean-square norm of the loop output hidden state, averaged over the batch and sequence dimensions:

$$\text{ResNorm}^{(t)} = \frac{1}{BT} \sum_{b=1}^B \sum_{i=1}^T \|h_{L,b,i}^{(t)}\|_2.$$

Unless otherwise specified, we report the norm of the first loop output.

The gradient L2 norm is computed over all parameters of the first FFN block:

$$\text{GradNorm} = \left(\sum_{p \in \mathcal{P}_{\text{FFN}_1}} \|\nabla_p \mathcal{L}\|_2^2 \right)^{1/2}.$$

We record this value before global gradient clipping.

A.3 Architecture Details

Backbone Network Architecture

All model variants share a common set of architectural choices. We use Rotary Positional Embeddings (RoPE) [Su et al., 2023] with base $\theta = 10000$ and no learnable positional embeddings. All

normalization is performed by a parameter-free RMSNorm (i.e. $\text{norm}(\mathbf{x}) = \mathbf{x}/\|\mathbf{x}\|_{\text{rms}}$ with no affine parameters). Attention uses QK-Norm [Henry et al., 2020]: after projecting queries and keys, each head vector is normalized before computing attention weights, which improves training stability. The FFN uses a ReLU² activation [Zhang et al., 2024] with an expansion ratio of 4. Logits are soft-capped via $15 \tanh(\ell/15)$ before computing cross-entropy loss, following Team et al. [2024]. The token embedding matrix and the language-model head are *untied* (separate parameters). No bias terms are used in any linear layer. Model dimensions are derived from a single depth hyperparameter:

$$d_{\text{model}} = 64 \times \text{depth}, \quad H = \lceil d_{\text{model}}/128 \rceil, \quad L = \text{depth}, \quad (5)$$

where H is the number of query heads and L is the number of unique Transformer blocks. The vocabulary size is padded to the nearest multiple of 64 for computational efficiency.

The total parameter count (standard MHA, padded vocab size V) is:

$$N = 2Vd_{\text{model}} + 12Ld_{\text{model}}^2. \quad (6)$$

Note that increasing the loop count K adds compute but *no* additional parameters, since the L blocks are reused across all K iterations.

Attention Variants

We implement three orthogonal attention design axes, each selectable independently: the KV projection scheme (`attn_type`), the head-sharing ratio (GQA), and the context window size (`window_pattern`).

Standard attention with Group-Query Attention (`attn_type='full'`). Each attention layer projects the input into H_q query heads and H_{kv} key/value heads:

$$\mathbf{W}_Q \in \mathbb{R}^{d \times H_q d_h}, \quad \mathbf{W}_K \in \mathbb{R}^{d \times H_{kv} d_h}, \quad \mathbf{W}_V \in \mathbb{R}^{d \times H_{kv} d_h}, \quad \mathbf{W}_O \in \mathbb{R}^{d \times d},$$

where $d_h = d_{\text{model}}/H_q$ is the per-head dimension. RoPE is applied to each query and key head vector. After RoPE, a parameter-free RMSNorm (QK-Norm) is applied independently to each query and key head vector before computing attention weights. This normalizes the pre-softmax dot products and improves training stability without introducing learnable parameters.

Group-Query Attention requires $H_{kv} \mid H_q$: each of the H_{kv} KV heads is broadcast to H_q/H_{kv} query heads. Setting $H_{kv} = H_q$ recovers standard Multi-Head Attention (MHA); setting $H_{kv} = 1$ gives Multi-Query Attention (MQA). The per-block parameter count under GQA is $(10 + 2r) d_{\text{model}}^2$ where $r = H_{kv}/H_q$, compared to $12 d_{\text{model}}^2$ for MHA. We set $H_{kv} = H_q$ by default and apply GQA selectively as a KV-cache memory reduction technique.

Multi-head Latent Attention (`attn_type='mla'`). To further reduce KV-cache memory during inference, we implement a low-rank KV compression scheme. Queries are projected in the standard way. For keys and values, a shared down-projection first compresses the input to a low-dimensional latent:

$$\mathbf{c}_{kv} = \text{norm}(\mathbf{x} \mathbf{W}_{\text{down}}), \quad \mathbf{W}_{\text{down}} \in \mathbb{R}^{d \times R}, \quad (7)$$

where R is the KV latent rank (default $R = 128$) and norm is the parameter-free RMSNorm. The latent is then expanded back to full KV representations via separate up-projections:

$$\mathbf{K} = \mathbf{c}_{kv} \mathbf{W}_K^\uparrow, \quad \mathbf{V} = \mathbf{c}_{kv} \mathbf{W}_V^\uparrow, \quad \mathbf{W}_K^\uparrow, \mathbf{W}_V^\uparrow \in \mathbb{R}^{R \times H_{kv} d_h}.$$

RoPE and QK-Norm are applied to the expanded \mathbf{Q} and \mathbf{K} as in the standard case. The RMSNorm on \mathbf{c}_{kv} decouples the gradient flow between the down-projection and the two up-projections, improving optimization stability. The KV cache stores the expanded \mathbf{K} and \mathbf{V} tensors (not the compressed latent), preserving the same inference interface as the standard attention. The per-block attention parameter count for MLA is $d^2 + dR + 2RH_{kv}d_h + d^2$, and the KV-cache footprint per token per layer is reduced by a factor of $H_{kv}d_h/R$ compared to MHA.

Sliding Window Attention (`window_pattern`). Independently of the KV projection scheme, each layer’s attention span can be restricted to a local window via the `window_pattern` string. The pattern is a sequence of characters (L or S) that is tiled across the L layers:

- L (long): full causal context, $w = T$ (no restriction).
- S (short): local causal window of size $w = \lfloor T/4 \rfloor$.

The final layer is always forced to full context regardless of the pattern, ensuring that the last-layer representations integrate global information. Concretely, for query position i and key position j , the attention mask enforces both the causal constraint ($j \leq i$) and, when applicable, the window constraint ($i - j < w$). When $w = T$ (full context), the fast `is_causal=True` path of `scaled_dot_product_attention` is used; otherwise an explicit Boolean mask is constructed and passed to the attention kernel.

Weight Initialization

Table 3: Weight initialization scheme.

Parameter	Distribution	Scale
Token embedding <code>wte</code>	Normal	$\sigma = 1.0$
LM head <code>lm_head</code>	Normal	$\sigma = 0.001$
$\mathbf{W}_Q, \mathbf{W}_K, \mathbf{W}_V, \text{FFN}_{\text{fc}}$	Uniform	$[-s, s], s = \sqrt{3/d_{\text{model}}}$
Output projections $\mathbf{W}_O, \text{FFN}_{\text{proj}}$	Constant	0

The Uniform bound $s = \sqrt{3/d_{\text{model}}}$ achieves the same standard deviation as $\mathcal{N}(0, 1/d_{\text{model}})$. Initializing output projections to zero ensures that the residual contribution of each block is zero at the start of training.

A.4 Experiments Details

We evaluate our models on four complementary metrics. Unless otherwise noted, all evaluations are run with `bfloat16` mixed precision under `torch.amp.autocast` and with a per-device batch size of 4 sequences.

Bits-per-Byte (BPB)

During training we track validation BPB every 250 steps as the primary per-training-step signal. BPB is a tokenization-independent compression metric defined as

$$\text{BPB} = \frac{\sum_t \ell_t}{\log 2 \cdot \sum_t b_t}, \quad (8)$$

where ℓ_t is the per-token cross-entropy loss (in nats) and b_t is the number of UTF-8 bytes that token t represents. Special tokens (e.g. `<|im_start|>`) contribute $b_t = 0$ and are therefore excluded from both numerator and denominator, as are any positions masked with `ignore_index = -1`. This normalization makes BPB comparable across models trained with different vocabulary sizes. BPB is reported on both the training corpus and the held-out validation shard (the final Parquet shard).

CORE Benchmark

CORE is an aggregate benchmark sourced from the DCLM evaluation suite. It covers a diverse set of language understanding tasks grouped into three evaluation types:

- **Multiple-choice** (`multiple_choice`): Each item has a shared context (query) and several candidate continuations. The model scores each candidate by computing the mean cross-entropy loss over the *continuation-only* tokens (i.e. the tokens that differ across choices; the common prefix is not scored). The candidate with the lowest loss is selected as the prediction.
- **Schema** (`schema`): Each item has multiple possible contexts paired with a shared continuation. The model scores each context by computing the mean cross-entropy loss over the shared *suffix* tokens. The context with the lowest loss is selected.

- **Language modeling** (`language_modeling`): Each item has a single context and a target continuation. The model computes the mean cross-entropy loss over the continuation tokens only (identified via a prefix-length comparison). Correct prediction requires the loss to fall below a threshold implicitly defined by the accuracy computation.

All three types use few-shot prompting; the number of in-context examples per task is fixed by the benchmark configuration. Few-shot examples for each query are sampled without replacement using a per-example random seed ($1234 + \text{idx}$), independently of the global data shuffle. Before evaluation, the full dataset for each task is shuffled with a fixed seed (1337) for reproducibility. We use all examples (i.e. `max_per_task = -1`) for final evaluations; during training we subsample to at most 500 examples per task for efficiency.

The raw per-task accuracy a is converted to a *centered accuracy*:

$$\tilde{a} = \frac{a - a_{\text{rand}}}{1 - a_{\text{rand}}}, \quad (9)$$

where a_{rand} is the random-baseline accuracy for that task (provided by the benchmark metadata). The overall **CORE metric** is the mean of all per-task centered accuracies.

WikiText-2 Perplexity

We evaluate standard language-model perplexity on the WikiText-2 validation set:

$$\text{PPL} = \exp\left(\frac{1}{N} \sum_{t=1}^N \ell_t\right), \quad (10)$$

where ℓ_t is the per-token NLL at position t and N is the total number of non-masked tokens. WikiText-2 PPL is always reported alongside CORE and BPB in post-training evaluations.

Test-Time Compute Budget Evaluation

A central aim of this work is to show that inference-time compute can be traded for improved performance by adjusting the loop count K without reloading or modifying model weights. To characterise this behaviour, we run a *budget evaluation* for every checkpoint: the model is evaluated at $K \in \{1, 3, 6, 9, 12\}$ loop iterations in a single pass, logging all four metrics (BPB, CORE, WikiText-2 PPL) at each budget point. Results are recorded with K as the x-axis, yielding a compute-performance curve for each model. This protocol enables direct comparison of a model at its native training compute versus cheaper ($K = 1$) or more expensive ($K = 12$) inference settings, as well as cross-model comparisons at equal inference cost.

Benchmark Statistics

In addition to language-modeling metrics, we evaluate each trained model on a set of standard downstream benchmarks. Table 4 summarizes the benchmarks and the number of in-context examples used for evaluation. We use 0-shot evaluation for LAMBADA OpenAI [Paperno et al., 2016, Radford et al., 2019] and OpenBookQA [Mihaylov et al., 2018], and 10-shot evaluation for PIQA [Bisk et al., 2020], HellaSwag [Zellers et al., 2019], ARC-Easy [Clark et al., 2018], and ARC-Challenge [Clark et al., 2018]. All downstream results are reported as accuracy.

B Broader Impacts

This work is primarily methodological and studies how to improve the training stability of looped language models without increasing the number of learnable parameters. A potential positive impact is that more stable and parameter-efficient architectures may help reduce the cost of training and deploying language models, making test-time compute adjustment more accessible. By allowing performance to be traded against inference-time computation through the number of loop iterations, such models may also provide more flexible deployment options under different resource constraints.

At the same time, improvements in language-model training efficiency can have broader dual-use implications. More stable and compute-adaptive language models may lower the barrier to training

Benchmark	Shots	Task type
LAMBADA OpenAI	0-shot	Cloze-style language understanding
OpenBookQA	0-shot	Multiple-choice open-book science question answering
PIQA	10-shot	Physical commonsense reasoning
HellaSwag	10-shot	Commonsense sentence completion
ARC-Easy	10-shot	Multiple-choice science question answering
ARC-Challenge	10-shot	Multiple-choice science question answering

Table 4: Downstream evaluation benchmarks used in this work. The “Shots” column indicates the number of in-context examples used during evaluation. All benchmarks are evaluated by selecting the answer with the highest model likelihood, unless otherwise specified. We report accuracy for all downstream benchmarks.

capable generative systems, which could be misused for spam, misinformation, or other harmful content generation if deployed without safeguards. In addition, although looped models do not increase parameter count, using more loop iterations at inference increases computation and energy consumption. Like other language models trained on web-scale corpora, models based on this architecture may also inherit biases, factual errors, or harmful associations from the training data.

Our experiments are conducted on publicly available datasets and standard academic benchmarks, and this work does not release a high-risk pretrained model. Nevertheless, future applications of this architecture should be accompanied by appropriate safety evaluations, bias and robustness analyses, content-misuse mitigation, and transparent reporting of compute and energy costs.

B.1 Existing Assets

We use publicly available benchmark datasets and standard open-source software libraries. The original sources of the datasets and any external code or models are cited in the main paper. We use these assets only for academic research and do not redistribute third-party datasets, models, or code.

Asset	Usage	License
FineWeb-Edu	Pretraining data	ODC-BY-v1.0
WikiText-2	Perplexity evaluation	CC-BY-SA-4.0
PIQA	Evaluation benchmark	Not specified
HellaSwag	Evaluation benchmark	MIT
ARC	Evaluation benchmark	Not specified
OpenBookQA	Evaluation benchmark	Not specified
Qwen3 tokenizer	Tokenizer	Apache-2.0
nanochat	Code reference	MIT

Table 5: Existing assets used in this work.